APPLIED PHYSICS

Skin-like low-noise elastomeric organic photodiodes

Youngrak Park[1], Canek Fuentes-Hernandez[1]*†, Kyungjin Kim[2]‡, Wen-Fang Chou[1], Felipe A. Larrain[1]§, Samuel Graham[2], Olivier N. Pierron[2], Bernard Kippelen[1]*

Stretchable optoelectronics made of elastomeric semiconductors could enable the integration of intelligent systems with soft materials, such as those of the biological world. Organic semiconductors and photodiodes have been engineered to be elastomeric; however, for photodetector applications, it remains a challenge to identify an elastomeric bulk heterojunction (e-BHJ) photoactive layer that combines a low Young's modulus and a high strain at break that yields organic photodiodes with low electronic noise values and high photodetector performance. Here, a blend of an elastomer, a donor-like polymer, and an acceptor-like molecule yields a skin-like e-BHJ with a Young's modulus of a few megapascals, comparable to values of human tissues, and a high strain at break of 189%. Elastomeric organic photodiodes based on e-BHJ photoactive layers maintain low electronic noise current values in the tens of femtoamperes range and noise equivalent power values in the tens of picowatts range under at least 60% strain.

INTRODUCTION

As technology evolves, the demand for interfaces that connect the digital and physical worlds continues to increase. Wearables, the Internet of Things, soft robotics, and many other emerging technologies use flexible optoelectronics to develop intelligent surfaces that combine sensors, computation, and communication. However, when objects are soft, their surface deforms under stress, i.e., when they experience strain, and flexibility is no longer sufficient to ensure mechanical compliance or ergonomics.

Photodetectors are an important class of sensors that generally benefit from having large photoactive areas that are sensitive to strain. Since the surface of soft objects experiences strain under normal conditions, stretchable photodetectors are expected to provide a roughed sensor platform that could find multiple applications for skin-mounted health monitors such as photoplethysmogram sensors (*1*, *2*), sensors mounted on the surface of living organisms such as plants for smart agriculture, sensors for artificial skin (*3*, *4*) and soft robotics (*5*–*7*), electronic eyes on curvilinear surfaces (*8*), and sensors for asset tracking, gesture, and motion recognition (*9*) mounted on packaging, produce, furniture, or textiles among many others.

Device architectures that heterogeneously integrate rigid optoelectronics with soft and stretchable substrates by using strain relief features such as stretchable interconnect remain the most common approach to achieve stretchable optoelectronics (*6*, *10*). The complex fabrication of such stretchable optoelectronics could be eased by the use of elastomeric semiconductors, but reports on such materials remain scarce. By elastomeric, it is meant that semiconductor layers have viscoelastic properties, with a low Young's modulus and a large strain at break.

Organic materials provide an attractive route to achieve elastomeric semiconductors because their properties can be engineered by design (*11*). For instance, conjugated polymers with long side-chain groups can dissipate strain energy through the amorphous regions while preserving the integrity of charge transport through the more ordered regions (*12*–*14*). Another approach is to blend a polymer semiconductor with a soft elastomer matrix [e.g., polystyrene-block-poly(ethylene-ran-butylene)-block-polystyrene, SEBS] to form self-assembled polymer nanofibers inside the elastomer. Such an approach yielded elastomeric organic field-effect transistors with field-effect charge mobility values up to 1 $cm^2\ V^{-1}\ s^{-1}$ at a strain value of 100% (*15*).

Despite recent progress in the development of elastomeric semiconductors, organic photodiodes with elastomeric bulk heterojunction (e-BHJ) photoactive layers showing a small electronic noise have not been demonstrated yet. BHJ photoactive layers require a blend of π donor– and π acceptor–like molecules forming a BHJ morphology to facilitate exciton dissociation and enable efficient photogeneration of charge carriers and efficient carrier extraction. To date, most BHJs cannot be considered skin-like elastomers because even if some are somewhat stretchable, they have large Young's modulus (E) values in the range between ca. 200 MPa and 1 GPa (*16*–*18*), which are at least one order of magnitude larger than typical values for human tissues (<30 MPa) (*19*–*21*) and, with a few exceptions (*22*, *23*), strain at break values smaller than 10% (*17*).

Despite showing limited mechanical properties, stretchable organic photodiodes (OPDs) based on these BHJs have been demonstrated in the context of photovoltaics (*18*) by using prestrained substrates (*24*), moderately stretchable BHJ (*23*, *25*), or all-polymer BHJ (*26*, *27*). To date, stretchable OPDs used in photovoltaics do not retain their performance under illumination beyond strain values ca. 50%, with one notable exception sustaining 100% strain but having a high E of 5.5 GPa (*23*). Recently, a ternary blend of polydimethylsiloxane (PDMS), a donor polymer, and a nonfullerene acceptor yielded a high E value of 990 MPa, maintaining a normalized power conversion efficiency of 86.7% up to a strain of 20% (*28*). Because these devices were tested for photovoltaic applications, their characteristics in the dark or at low irradiance values were not reported.

In the context of photodetection, stretchable OPDs have been demonstrated using conventional BHJ materials by laminating complete devices onto a prestrained substrate. These stretchable OPDs

[1]Center for Organic Photonics and Electronics (COPE), School of Electrical and Computer Engineering, Georgia Institute of Technology, Atlanta, GA 30332, USA. [2]George W. Woodruff School of Mechanical Engineering, Georgia Institute of Technology, Atlanta, GA 30332, USA.
*Corresponding author. Email: c.fuentes@northeastern.edu (C.F.-H.); kippelen@gatech.edu (B.K.)
†Present address: Department of Electrical and Computer Engineering, Northeastern University, MA 02115, USA.
‡Present address: Department of Mechanical Engineering, University of Connecticut, Storrs, CT 06269, USA.
§Present address: Facultad de Ingeniería y Ciencias, Universidad Adolfo Ibáñez, Santiago 7941169, Chile.

were tested under compressive strain in the context of pulse oximetry (*2*, *3*), but the characterization of their performance parameters was limited to measurements of their dark current density values (in the range of 0.1 to 10 μA cm^{-2} under reverse bias) and their responsivity ($\mathfrak{R}_{max}$ = 0.144 A W^{-1}) under 100 mW cm^{-2} simulated solar illumination (*2*). As recently discussed (*29*, *30*), accurate characterization of the performance parameters of a photodetector requires direct measurement of its electronic noise in the dark, as well as a direct measurement of its noise equivalent power (NEP). The electronic noise is defined as the root mean square value (I_{rms}) of the current fluctuations ($I_{dark}[t]$) around the average current value measured in the dark ($\bar{I}_{dark}$). Values of I_{rms} are not expected to be limited by shot noise current values when electric measurements are carried out at low-frequency bandwidth values and, consequently, cannot be accurately calculated from steady-state dark current versus voltage characteristics typically reported in the literature. The NEP is defined as the average optical power ($\bar{\phi}$) required to generate an average photocurrent ($\bar{I}_{ph}$) with an amplitude that is equal to I_{rms}, i.e., with a signal-to-noise ratio (SNR = $\bar{I}_{ph}/I_{rms}$) of 1. Measured NEP values allow the specific detectivity to be calculated as $D^* \equiv \sqrt{A_{PD}B}/\text{NEP}$, where A_{PD} is the device area and B is the measurement bandwidth. D^* is the most common performance metric used to compare different photodetector performance, but the use of approximations in calculating its value can be inaccurate. This is particularly true if the responsivity, i.e., the ratio $\bar{I}_{ph}/\bar{\phi}$, measured at a high optical power is assumed to be independent of the magnitude of the optical power (*29*, *30*). For these reasons, calculating performance metrics from reported steady-state current values and measurements at high optical power values is unreliable.

Here, we report that a blend of the elastomer SEBS, the donor polymer poly(3-hexylthiophene-2,5-diyl) (P3HT), and the acceptor Indene-C60 bisadduct (ICBA) yields a skin-like e-BHJ with a low E and a high strain at break, comparable to those of SEBS. Although pristine P3HT:ICBA BHJ layers are not elastomeric, this BHJ has enabled OPDs with a level of performance that is comparable to that of low-noise silicon photodiodes (SiPDs) (*29*). Here, we demonstrate that stretchable OPDs using this previously unidentified e-BHJ show dark current density values smaller than 600 pA cm^{-2} under reverse bias, but more importantly from a photodetector perspective, a measured median root mean square electronic noise in the tens of femtoampere range and measured NEP values at 653 nm between 13 and 24 pW at strain values up to 60%, yielding D^* values in the 10^{10} Jones range.

RESULTS

Samples of SEBS:P3HT:ICBA with different compositions were initially prepared and evaluated in a photodiode device architecture. On the basis of a preliminary screening of their optical and electrical properties, films with a SEBS:P3HT:ICBA (2:1:1 by weight) composition were found to yield the best performance. Hence, the mechanical and electrical properties of films and devices made with this particular composition are discussed below.

First, the mechanical properties of freestanding films of SEBS:P3HT:ICBA (2:1:1 by weight), hereon referred to as e-BHJ, were characterized and compared with those of P3HT:ICBA (1:1 by weight), hereon referred to as reference-BHJ (r-BHJ), and pristine SEBS. Figure 1A shows the chemical structure of these materials. Uniaxial tensile tests were performed to plot stress (σ)–strain (ε) curves (Fig. 1B), and the corresponding E and strain at break values were derived (Fig. 1C). E values are in the range from 259 to 264 MPa for r-BHJ films. The shape of the stress-strain plot derived from these measurements and, consequently, E values derived from them highly depend on stress-strain definitions (e.g., engineering stress-strain, true stress-engineering strain, and true stress-strain defined in Materials and Methods) for e-BHJ and SEBS due to the hyperelastic deformation (fig. S1A). Regardless of the definition used, E values are between 2.4 and 6.9 MPa for e-BHJ films and between 0.8 and 2.4 MPa for SEBS films; this is ca. two orders of magnitude smaller than in r-BHJ. In addition, the strain at break increases from 6% in r-BHJ films to 189% (inset of Fig. 1B) in e-BHJ films, similar to values measured in pristine SEBS films (table S1) and comparable to those of human tissues (*20*).

Having demonstrated skin-like mechanical properties, e-BHJ films were further investigated by incorporating them into an OPD geometry fabricated on a rigid substrate (inset Fig. 2A). Figure 2A (top)

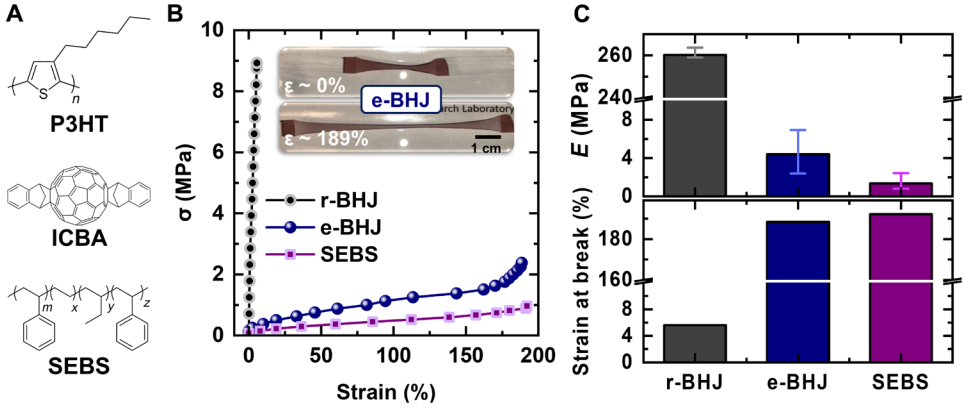

Fig. 1. Mechanical characterization of freestanding films. (**A**) Chemical structure of materials used in P3HT:ICBA (1:1) (r-BHJ) and SEBS:P3HT:ICBA (2:1:1) (e-BHJ) film. (**B**) Stress (σ) versus strain (ε) behavior of r-BHJ, e-BHJ, and SEBS from the uniaxial tensile test. A photograph of the relaxed and strained (189%) e-BHJ film [(B), inset]. (**C**) Range of Young's moduli (E) using different stress-strain definitions. The error bars represent the minimum and maximum bounds of E (top). Strain at break compared to the initial length (bottom). Photo credit: Youngrak Park, Georgia Institute of Technology.

shows that, under reverse bias, the values of the voltage (V)–dependent dark current density (J_{dark}) of the champion device are at least four orders of magnitude smaller than those previously reported on stretchable OPDs (*2*). Figure 2A (bottom) shows that the distribution of measured I_{rms} values, with a median of 72 fA at $V = 0$ V and at a measurement bandwidth of $B = 1.5$ Hz, is comparable to that of low-noise SiPDs (Hamamatsu S1133 series) and state-of-the-art P3HT:ICBA OPDs recently reported (*29*).

Figure S2 shows that a direct measurement of the NEP (653 nm, 1.5 Hz) yields a value of 39 pW at 0 V. Note that this value is larger than the value of $NEP_{extrapolated} = 10$ pW calculated by extrapolating the photocurrent to the median I_{rms} using a $\mathfrak{R}$(653 nm) of 7.5 mA W^{-1} derived from the photocurrent slope at optical power values between 1 nW and 10 μW (Fig. 2B). This discrepancy arises because $\mathfrak{R}$ decreases as the optical power approaches the NEP, reaching a value of 1.9 mA W^{-1} at the NEP. Similar behavior has been observed in low-noise SiPDs and OPDs and has been attributed to the presence of traps (*30*). Measured NEP values yield a D^* (0.1 cm^2, 1.5 Hz) of 1.0×10^{10} Jones at 653 nm. Figure 2C (top) shows that, for average optical power values of 27 μW, $\mathfrak{R}$(560 nm) reaches a peak value of 71 mA W^{-1}, which is significantly larger than at the NEP. Assuming that $\mathfrak{R}$(653 nm) losses (ca. 75%) at the NEP are similar at other wavelengths, a peak D^* value of 5.3×10^{10} Jones at 560 nm is estimated (Fig. 2C, bottom).

We now demonstrate the use of e-BHJ films to realize elastomeric OPDs, hereon referred to as e-OPD. Figure 3A shows a schematic of

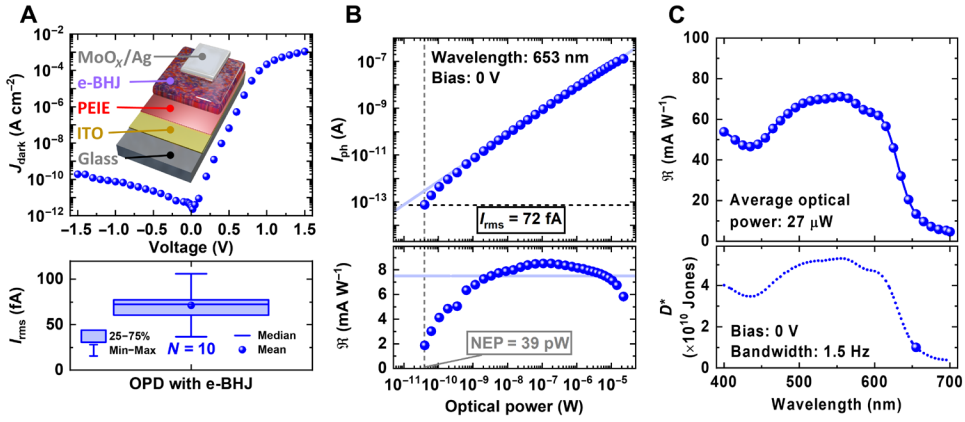

Fig. 2. Photodetector characterization of OPD with e-BHJ on a rigid substrate. (**A**) Dark current density (top) and root mean square noise box plot (N = number of data points) (bottom). The device structure of OPD [(A), inset]. (**B**) Optical power–dependent photocurrent (top) and responsivity (bottom). (**C**) Spectral responsivity (top) and specific detectivity (bottom); symbols correspond to measured data points.

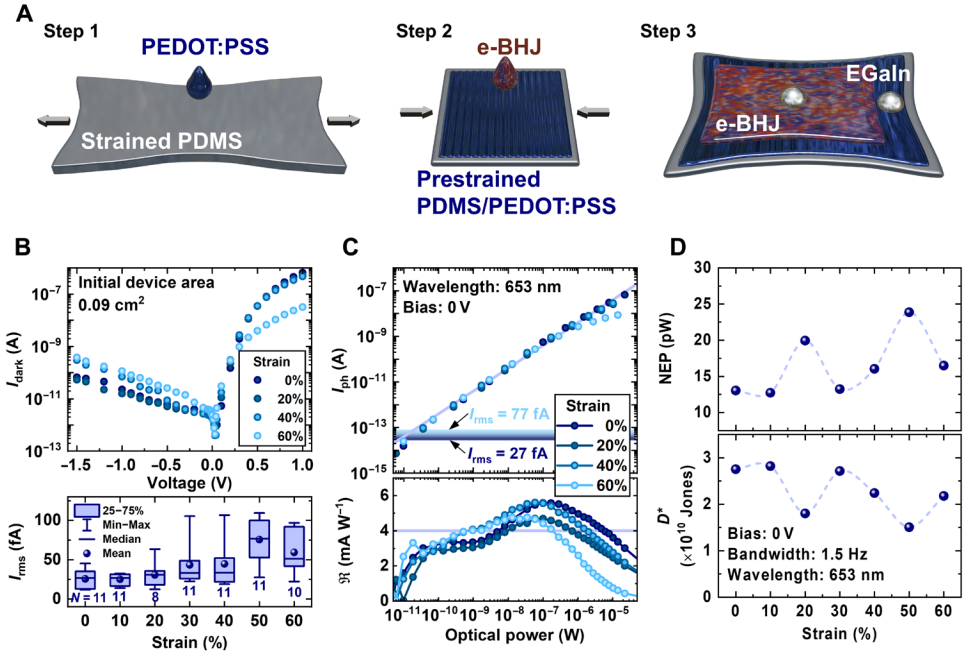

Fig. 3. Photodetector characterization of e-OPD under different strains. (**A**) Schematics of the fabrication process. (**B**) Dark current (top) and root mean square noise box plot (bottom). (**C**) Optical power–dependent photocurrent (top) and responsivity (bottom). (**D**) NEP (top) and specific detectivity (bottom).

the fabrication process and structure of e-OPD with an e-BHJ. A key difference with respect to previous work is that, in the first step, only poly(3,4ethylenedioxythiophene):poly(styrenesulfonate) (PEDOT:PSS) was spin-coated directly onto a 30% prestrained PDMS film. In the second step, the substrate was released, and the e-BHJ was spin-coated on top of the buckled PDMS/PEDOT:PSS substrate. In such geometry, the e-BHJ experiences not only flexural deformation but also elastic deformation. Last, a drop of eutectic gallium-indium (EGaIn) was used as top electrode. The photodetector characteristics of e-OPDs were then measured as a function of strain. Note that the e-OPD was released to 0% strain between different strain values. Figure 3B (top) shows that I_{dark} versus V characteristics of e-OPDs are comparable to those measured on OPDs with an e-BHJ on rigid glass substrates and remain comparable under reverse bias up to 60% strain. Furthermore, Fig. 3B (bottom) shows that the distribution of I_{rms} values is similar to those found on OPDs with e-BHJ on a rigid substrate, with median values of 27 fA in unstrained e-OPD and 51 fA at 60% strain. Figure 3C shows that up to a strain value of 60%, the photocurrent varies approximately linearly with optical power for values between 1 nW and 1 μW, yielding a $\mathfrak{R}$(653 nm) of 4 mA W^{-1}. Deviations at optical power values larger than 1 μW are caused by the increased series resistance when e-OPDs are subjected to 60% strain (Fig. 3B, top). At values below 100 pW, $\mathfrak{R}$(653 nm) decreases as the optical power approaches the NEP. Figure S3 shows that unstrained e-OPDs yield an NEP value of 13 pW. Figure 3D (top) shows that NEP values (653 nm, 1.5 Hz) at 0 V are in the range between 13 and 24 pW for e-OPDs strained up to 60%. These values are consistent with values measured on rigid OPDs with an e-BHJ and demonstrate that e-OPDs can sustain up to 60% strain without substantial degradation, yielding an average D^* value of 2.3×10^{10} Jones (Fig. 3D, bottom) at 653 nm.

Beyond strain values of 60%, the e-OPDs failed. As shown in fig. S4B, this is because the normalized resistance (R/R_0) of as-deposited and prestrained PDMS/PEDOT:PSS increases rapidly when the applied strain surpasses the PDMS strain used during PEDOT:PSS deposition. However, it was found that prestrained PDMS/PEDOT:PSS/e-BHJ films can sustain substantially larger strain values. These data support that failure of e-OPDs beyond 60% strain is caused by failure of the 30% prestrained PDMS/PEDOT:PSS electrode rather than the e-BHJ layer. To further confirm this, e-OPDs were fabricated on 60% prestrained PDMS/PEDOT:PSS electrodes. Figure S4C (top) shows that the I_{dark} versus V characteristics of e-OPDs are even superior to those found on e-OPDs shown in Fig. 3B (top), as they sustain strain values up to 100% without substantial degradation. Furthermore, the distribution of I_{rms} values shown in fig. S4C (bottom) remains similar to those found on rigid OPDs with an e-BHJ and e-OPDs shown in Fig. 3B (bottom), with median values between 30 and 38 fA for strain values up to 100%.

Last, we investigated the response time of e-OPD by connecting them to a transimpedance amplifier circuit with a 3-dB bandwidth of 530 kHz and by measuring their response time. As shown in Fig. 4A, response time values ranged from 60 to 79 μs up to 50% of strain, then doubled to 142 μs at 60% strain. This increase is correlated with an increased resistor-capacitor (RC) time constant due to the increased resistance of prestrained PDMS/PEDOT:PSS, as shown in fig. S4B. Figure 4B shows that a 3-dB normalized responsivity bandwidth of 7 kHz is maintained up to ca. 50% of strain and falls to 1 kHz at 60% strain. As previously discussed (*29*, *31*), these 3-dB bandwidth values are sufficiently high for the range of applications described in the Introduction.

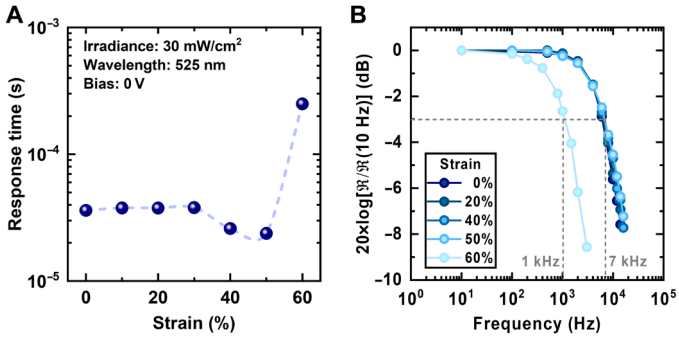

Fig. 4. Response time of e-OPD under different strains. (**A**) Ten to 90% response time. (**B**) Frequency-dependent normalized responsivity.

DISCUSSION

This study demonstrates that stretchable OPDs based on e-BHJs with skin-like mechanical properties can yield a low electronic noise and a high level of performance. Tensile testing on the freestanding film of e-BHJ yields a tensile modulus of 2.4 MPa and a strain at break of 189%, which are within the range of values found in human tissue. Using an e-BHJ, OPDs fabricated on a rigid substrate show low electronic noise values in the tens of femtoampere range and a measured NEP of 39 pW at 653 nm and a corresponding peak D^* value of 5.3×10^{10} Jones at 560 nm. The NEP value of e-BHJ OPDs is larger than that achieved by state-of-the-art P3HT:ICBA OPDs, because devices with an e-BHJ show a smaller responsivity. This is in part because the addition of SEBS at 50 weight % (wt %) reduces the absorption of light in an e-BHJ by at least 50% when compared to a pristine BHJ. In addition, there is a significant reduction of the responsivity values when the optical power is smaller than around 1 nW, which may be due to the presence of traps. Despite these shortcomings, e-OPD based on prestrained PEDOT:PSS and EGaIn electrodes exhibit NEP values in the tens of picowatts range and D^* values in the 10^{10} Jones range at 653 nm and retain these values up to a strain of at least 60%. While it is clear that further optimization of material composition, selection of donor and acceptor moieties in the BHJs, and device geometry could be carried out, these results constitute a proof-of-principle demonstration of low-noise e-OPDs that combine the mechanical properties of skin-like elastomers while approaching the remarkable performance of rigid organic photodetectors. This unique combination of properties could enable a myriad of new applications by enabling the seamless integration of optoelectronics with soft materials.

MATERIALS AND METHODS

Fabrication of freestanding films

Glass substrates were cleaned in sequential ultrasonic baths of Liquinox detergent in deionized water, deionized water, acetone, and isopropanol. To create a sacrificial layer, polyethylenimine ethoxylated (PEIE) (Sigma-Aldrich) dissolved in H_2O at a concentration of 37 wt % was further diluted with 2-methoxyethanol to a concentration of 18 wt %. This PEIE solution was then spin-coated on a cleaned glass substrate at 1000 revolutions per minute (rpm) for 1 min and annealed on a hot plate at 100°C for 10 min. The PEIE-coated substrate was then transferred into an N_2-filled glove box for further processing. The r-BHJ and e-BHJ consist of a blend of regioregular P3HT (Rieke Metals) with ICBA (Nano-C) at a 1:1 weight ratio and a blend of

SEBS (Asahi Kasei Corporation, H1221):P3HT:ICBA at a 2:1:1 weight ratio, respectively. Chlorobenzene solutions of the r-BHJ, e-BHJ, and pristine SEBS at a concentration of 80 mg/ml were stirred overnight at 70°C on a hot plate in the nitrogen-filled glove box and cooled down at room temperature before they were spin-coated onto the glass/indium tin oxide (ITO)/PEIE substrate at 800 rpm for 30 s. The resulting wet films were then slowly dried inside covered glass petri dishes for 3 hours. The sample was then thermally annealed on a hot plate at 150°C for 10 min. The thicknesses of the r-BHJ, e-BHJ, and SEBS freestanding films are 700 ± 2, 1000 ± 8, and 1683 ± 9 nm, respectively, measured with a scan area of 30 μm × 30 μm by atomic force microscopy (AFM). Each film was cut into an 8 mm × 38 mm strip, and each end of the film was gently pressed on the PDMS (Dow Corning Co., Sylgard 184) for van der Waals bonding to allow tensile testing. The freestanding films in the form of a strap were obtained by immersing the substrate in deionized water for 30 min to completely dissolve the PEIE underneath.

Fabrication of OPD with e-BHJ on a rigid substrate

Custom-patterned ITO-coated glass sheets with a sheet resistance of 12 to 15 ohms per square were used as a substrate for OPDs. The ITO substrate was cleaned in ultrasonic baths of Liquinox detergent in deionized water, deionized water, acetone, and isopropanol sequentially. PEIE dissolved in H_2O at a concentration of 37 wt % was further diluted with 2-methoxyethanol to a concentration of 0.3 wt %. The 0.3 wt % PEIE solution was then spin-coated on the ITO substrate at 5000 rpm for 1 min and annealed on a hot plate at 100°C for 10 min. The substrate was then transferred into an N_2-filled glove box for further processing. The r-BHJ consists of a blend of regioregular P3HT with ICBA at a 1:1 weight ratio. Elastomeric BHJ consists of P3HT:ICBA at a 1:1 weight ratio and SEBS at different weight ratios (e.g., 33, 50, and 67%) with respect to P3HT:ICBA. As defined here, the e-BHJ consists of SEBS:P3HT:ICBA at a 2:1:1 weight ratio. A chlorobenzene solution of the e-BHJ at a concentration of 40 mg/ml was stirred overnight at 70°C on a hot plate in the nitrogen-filled glove box and cooled down at room temperature before they were spin-coated onto the glass/ITO/PEIE substrate at 800 rpm for 30 s. The resulting wet films were then slowly dried in covered glass petri dishes for 3 hours. The sample was then thermally annealed on a hot plate at 150°C for 10 min. The thickness of the e-BHJ is 400 ± 8 nm, measured with a scan area of 30 μm × 30 μm by AFM. To provide effective hole collection, MoO_x/Ag (20/150 nm) was deposited on top of the substrate through a shadow mask with an effective area (A_{PD}) of 0.1 cm^2 at a pressure of $<5.0 \times 10^{-7}$ torr.

Fabrication of stretchable OPD (e-OPD)

Silicone elastomer PDMS was used as an elastomeric substrate for e-OPD. A sheet of PDMS (2 to 3 mm thick) with a curing agent/base ratio of 1:20 was obtained by curing in an oven at 60°C for 3 hours. Strained PDMS sheets (30 and 60%) were fixed on glass with paper clips. PEDOT:PSS (Ossila, PH1000) with 12 wt % of ethylene glycol and 15 wt % of capstone was spin-coated on the strained PDMS at 1000 rpm for 1 min and annealed on a hot plate at 100°C for 10 min. The thickness of the PEDOT:PSS deposited on glass is 392 ± 6 nm measured at three different spots by a profilometer. After releasing, by removing the paper clips from glass, the substrate was transferred into an N_2-filled glove box for further processing. A chlorobenzene solution of the e-BHJ with a concentration of 40 mg/ml was stirred overnight at 70°C on a hot plate in the nitrogen-filled glove box and cooled down at room temperature before it was spin-coated onto the prestrained PDMS/PEDOT:PSS at 800 rpm for 30 s. The resulting wet film was then slowly dried in a covered glass petri dish for 3 hours. The device was completed by placing a liquid metal alloy, EGaIn (Sigma-Aldrich), on top of e-BHJ through a PDMS mask to control the area.

Mechanical characterization

The mechanical properties of the r-BHJ, e-BHJ, and SEBS were determined in a portable tensile stage (TST350, Linkam Scientific). A uniaxial monotonic loading was applied to the film on the surface of water at a rate of 0.5% s^{-1} until failure occurred in the middle of the specimen. A custom-made mini water reservoir was used to float the film. A gauge length was calculated for the freestanding film between the two PDMS holders. The engineering stress, σ_{eng}, and strain, ε_{eng}, were obtained based only on the initial cross-sectional area, A_0, and gauge length, L_0, as

$$\sigma_{eng} = \frac{F}{A_0} \quad (1)$$

$$\varepsilon_{eng} = \frac{L - L_0}{L_0} \quad (2)$$

where F is the load measured and L is the elongated gauge length. The true stress, σ_{true}, and strain, ε_{true}, were derived based on the instantaneous cross-sectional area, A, at the gauge length L, assuming that the volume of the film was preserved with a Poisson's ratio of 0.5. The correlation between true stress-strain and engineering stress-strain can also be found. Therefore

$$\sigma_{true} = \frac{F}{A} = \frac{F\,L}{A_0 L_0} = \sigma_{eng}(1 + \varepsilon_{eng}) \quad (3)$$

$$\varepsilon_{true} = \ln\left(\frac{L}{L_0}\right) = \ln(1 + \varepsilon_{eng}) \quad (4)$$

Figure S1A illustrates a comparison of the stress-strain curve between engineering stress-strain (Eng.-Eng.), true stress-engineering strain (True-Eng.), and true stress strain (True-True) on the mechanical behavior of e-BHJ. The nonlinear stress-strain curves were fitted to a third-order polynomial equation, and the elasticity was calculated via the derivative of the third-order polynomial equation in fig. S1B.

Photodetector characterization

The dark current and electronic noise were measured using a Keithley 6430 electrometer as detailed in (*29*). In short, the current was recorded as a function of time using a LabVIEW program. The voltage was controlled manually to allow for the dark current to reach steady-state values. The root mean square electronic noise current was derived by calculating the square root of the mean square of the current residuals derived from estimating the average current over time by fitting the current transients to an exponential decay function. The effective bandwidth of these measurements was estimated to be 1.5 Hz by measuring the current-voltage characteristics and electronic noise of a 1-gigohm resistor.

Similarly, the transient current was measured by the same procedure outlined above to ensure the measurement of steady-state values. The photocurrent extracted by subtracting the fitted dark current from the measured transient current was generated as a function of optical power (laser diode with a wavelength of 653 nm) by changing the bias voltage on the laser diode (figs. S2 and S3). The NEP and D^* are defined as the optical power producing an SNR (SNR = I_{ph}/I_{rms}) of 1 and $\sqrt{A_{PD}B}$/NEP, respectively.

The spectral responsivity $\mathfrak{R}(\lambda)$ was measured by using a laser-driven light source (Energetiq EQ-99X) connected with a monochromator (CVI Spectral Products, CM110) to produce spectrally narrow (ca. 10-nm full width at half maximum) illumination. The

steady-state current at each wavelength was measured using the same electrometer and procedure previously described.

The response time and frequency response of the e-OPD were measured using a transimpedance amplifier. The photodetector current in response to light having a square pulse shape produced by a green light-emitting diode (LED) at 525 nm with an irradiance of 30 mW cm^{-2}, was passed through a transimpedance amplifier designed by an operational amplifier (Texas Instruments, TL082), with a feedback resistance of 3 kilohms and a capacitance of 100 pF. The output voltage was obtained by an oscilloscope (Rohde & Schwarz, RTO 1002). We define rise time as the response time it takes for the output signal to go from 10 to 90% of its steady-state on-current. The transient voltage amplitude of e-OPD at each frequency was normalized to the amplitude measured at 10 Hz by sweeping the LED light frequency to obtain normalized responsivity.

SUPPLEMENTARY MATERIALS

Supplementary material for this article is available at https://science.org/doi/10.1126/sciadv.abj6565

REFERENCES AND NOTES

1. Y. Khan, A. E. Ostfeld, C. M. Lochner, A. Pierre, A. C. Arias, Monitoring of vital signs with flexible and wearable medical devices. *Adv. Mater.* **28**, 4373–4395 (2016).
2. S. Park, K. Fukuda, M. Wang, C. Lee, T. Yokota, H. Jin, H. Jinno, H. Kimura, P. Zalar, N. Matsuhisa, S. Umezu, G. C. Bazan, T. Someya, Ultraflexible near-infrared organic photodetectors for conformal photoplethysmogram sensors. *Adv. Mater.* **30**, 1802359 (2018).
3. T. Yokota, P. Zalar, M. Kaltenbrunner, H. Jinno, N. Matsuhisa, H. Kitanosako, Y. Tachibana, W. Yukita, M. Koizumi, T. Someya, Ultraflexible organic photonic skin. *Sci. Adv.* **2**, e1501856 (2016).
4. N. Gogurla, B. Roy, K. Min, J. Y. Park, S. Kim, A skin-inspired, interactive, and flexible optoelectronic device with hydrated melanin nanoparticles in a protein hydrogel–elastomer hybrid. *Adv. Mater. Technol.* **5**, 1900936 (2020).
5. Y. Lee, J. Y. Oh, W. Xu, O. Kim, T. R. Kim, J. Kang, Y. Kim, D. Son, J. B.-H. Tok, M. J. Park, Z. Bao, T.-W. Lee, Stretchable organic optoelectronic sensorimotor synapse. *Sci. Adv.* **4**, eaat7387 (2018).
6. R.-H. Kim, D.-H. Kim, J. Xiao, B. H. Kim, S.-I. Park, B. Panilaitis, R. Ghaffari, J. Yao, M. Li, Z. Liu, V. Malyarchuk, D. G. Kim, A.-P. Le, R. G. Nuzzo, D. L. Kaplan, F. G. Omenetto, Y. Huang, Z. Kang, J. A. Rogers, Waterproof AlInGaP optoelectronics on stretchable substrates with applications in biomedicine and robotics. *Nat. Mater.* **9**, 929–937 (2010).
7. H. Lee, Z. Jiang, T. Yokota, K. Fukuda, S. Park, T. Someya, Stretchable organic optoelectronic devices: Design of materials, structures, and applications. *Mater. Sci. Eng.* **146**, 100631 (2021).
8. H. C. Ko, M. P. Stoykovich, J. Song, V. Malyarchuk, W. M. Choi, C.-J. Yu, J. B. Geddes Iii, J. Xiao, S. Wang, Y. Huang, J. A. Rogers, A hemispherical electronic eye camera based on compressible silicon optoelectronics. *Nature* **454**, 748–753 (2008).
9. D. Zhang, J. W. Park, Y. Zhang, Y. Zhao, Y. Wang, Y. Li, T. Bhagwat, W.-F. Chou, X. Jia, B. Kippelen, C. Fuentes-Hernandez, T. Starner, G. D. Abowd, OptoSense: Towards ubiquitous self-powered ambient light sensing surfaces. *In Prof. of ACM IMWUT* **4**, 1–27 (2020).
10. H. Zhang, J. A. Rogers, Recent advances in flexible inorganic light emitting diodes: From materials design to integrated optoelectronic platforms. *Adv. Opt. Mater.* **7**, 1800936 (2019).
11. J.-S. Kim, J.-H. Kim, W. Lee, H. Yu, H. J. Kim, I. Song, M. Shin, J. H. Oh, U. Jeong, T.-S. Kim, B. J. Kim, Tuning mechanical and optoelectrical properties of poly(3-hexylthiophene) through systematic regioregularity control. *Macromolecules* **48**, 4339–4346 (2015).
12. A. D. Printz, S. Savagatrup, D. J. Burke, T. N. Purdy, D. J. Lipomi, Increased elasticity of a low-bandgap conjugated copolymer by random segmentation for mechanically robust solar cells. *RSC Adv.* **4**, 13635–13643 (2014).
13. J. Y. Oh, S. Rondeau-Gagné, Y.-C. Chiu, A. Chortos, F. Lissel, G.-J. N. Wang, B. C. Schroeder, T. Kurosawa, J. Lopez, T. Katsumata, J. Xu, C. Zhu, X. Gu, W.-G. Bae, Y. Kim, L. Jin, J. W. Chung, J. B. H. Tok, Z. Bao, Intrinsically stretchable and healable semiconducting polymer for organic transistors. *Nature* **539**, 411–415 (2016).
14. S. Savagatrup, A. S. Makaram, D. J. Burke, D. J. Lipomi, Mechanical properties of conjugated polymers and polymer-fullerene composites as a function of molecular structure. *Adv. Funct. Mater.* **24**, 1169–1181 (2014).
15. J. Xu, S. Wang, G.-J. N. Wang, C. Zhu, S. Luo, L. Jin, X. Gu, S. Chen, V. R. Feig, J. W. F. To, S. Rondeau-Gagné, J. Park, B. C. Schroeder, C. Lu, J. Y. Oh, Y. Wang, Y.-H. Kim, H. Yan, R. Sinclair, D. Zhou, G. Xue, B. Murmann, C. Linder, W. Cai, J. B.-H. Tok, J. W. Chung, Z. Bao, Highly stretchable polymer semiconductor films through the nanoconfinement effect. *Science* **355**, 59–64 (2017).
16. S. Savagatrup, D. Rodriquez, A. D. Printz, A. B. Sieval, J. C. Hummelen, D. J. Lipomi, [70] PCBM and incompletely separated grades of methanofullerenes produce bulk heterojunctions with increased robustness for ultra-flexible and stretchable electronics. *Chem. Mater.* **27**, 3902–3911 (2015).
17. B. Roth, S. Savagatrup, N. V. de los Santos, O. Hagemann, J. E. Carlé, M. Helgesen, F. Livi, E. Bundgaard, R. R. Søndergaard, F. C. Krebs, D. J. Lipomi, Mechanical properties of a library of low-band-gap polymers. *Chem. Mater.* **28**, 2363–2373 (2016).
18. J. Qin, L. Lan, S. Chen, F. Huang, H. Shi, W. Chen, H. Xia, K. Sun, C. Yang, Recent progress in flexible and stretchable organic solar cells. *Adv. Funct. Mater.* **30**, 2002529 (2020).
19. M. A. F. Kendall, Y.-F. Chong, A. Cock, The mechanical properties of the skin epidermis in relation to targeted gene and drug delivery. *Biomaterials* **28**, 4968–4977 (2007).
20. C. T. McKee, J. A. Last, P. Russell, C. J. Murphy, Indentation versus tensile measurements of Young's modulus for soft biological tissues. *Tissue Eng. Part B Rev.* **17**, 155–164 (2011).
21. S. P. Lacour, G. Courtine, J. Guck, Materials and technologies for soft implantable neuroprostheses. *Nat. Rev. Mater.* **1**, 16063 (2016).
22. S. Chen, S. Jung, H. J. Cho, N.-H. Kim, S. Jung, J. Xu, J. Oh, Y. Cho, H. Kim, B. Lee, Y. An, C. Zhang, M. Xiao, H. Ki, Z.-G. Zhang, J.-Y. Kim, Y. Li, H. Park, C. Yang, Highly flexible and efficient all-polymer solar cells with high-viscosity processing polymer additive toward potential of stretchable devices. *Angew. Chem. Int. Ed.* **57**, 13277–13282 (2018).
23. L. Li, J. Liang, H. Gao, Y. Li, X. Niu, X. Zhu, Y. Xiong, Q. Pei, A solid-state intrinsically stretchable polymer solar cell. *ACS Appl. Mater. Interfaces* **9**, 40523–40532 (2017).
24. D. J. Lipomi, B. C.-K. Tee, M. Vosgueritchian, Z. Bao, Stretchable organic solar cells. *Adv. Mater.* **23**, 1771–1775 (2011).
25. J. W. Mok, Z. Hu, C. Sun, I. Barth, R. Muñoz, J. Jackson, T. Terlier, K. G. Yager, R. Verduzco, Network-stabilized bulk heterojunction organic photovoltaics. *Chem. Mater.* **30**, 8314–8321 (2018).
26. T. Kim, J.-H. Kim, T. E. Kang, C. Lee, H. Kang, M. Shin, C. Wang, B. Ma, U. Jeong, T.-S. Kim, B. J. Kim, Flexible, highly efficient all-polymer solar cells. *Nat. Commun.* **6**, 8547 (2015).
27. Y.-Y. Yu, C.-H. Chen, C.-C. Chueh, C.-Y. Chiang, J.-H. Hsieh, C.-P. Chen, W.-C. Chen, Intrinsically stretchable nanostructured silver electrodes for realizing efficient strain sensors and stretchable organic photovoltaics. *ACS Appl. Mater. Interfaces* **9**, 27853–27862 (2017).
28. Z. Wang, M. Xu, Z. Li, Y. Gao, L. Yang, D. Zhang, M. Shao, Intrinsically stretchable organic solar cells beyond 10% power conversion efficiency enabled by transfer printing method. *Adv. Funct. Mater.* **31**, 2103534 (2021).
29. C. Fuentes-Hernandez, W.-F. Chou, T. M. Khan, L. Diniz, J. Lukens, F. A. Larrain, V. A. Rodriguez-Toro, B. Kippelen, Large-area low-noise flexible organic photodiodes for detecting faint visible light. *Science* **370**, 698–701 (2020).
30. Y. Fang, A. Armin, P. Meredith, J. Huang, Accurate characterization of next-generation thin-film photodetectors. *Nat. Photonics* **13**, 1–4 (2019).
31. J. A. C. Patterson, D. C. McIlwraith, G.-Z. Yang, *A Flexible, Low Noise Reflective PPG Sensor Platform for Ear-Worn Heart Rate Monitoring*, paper presented at the 2009 Sixth International Workshop on Wearable and Implantable Body Sensor Networks, Berkeley, CA, USA, 3 to 5 June 2009.

Acknowledgments

Funding: This research was supported by the following funding sources: Department of the Navy, Office of Naval Research award nos. N00014-14-1-0580 and N00014-16-1-2520, through the MURI Center for Advanced Organic Photovoltaics (CAOP) (B.K., C.F.-H., and F.A.L.); Air Force Office of Scientific Research through award no. FA9550-16-1-0168. (B.K., C.F.-H., and W.-F.C.); Department of Energy/National Nuclear Security Administration (NNSA) award no. DE-NA0002576 through the Consortium for Nonproliferation Enabling Capabilities (CNEC) (Y.P. and W.-F.C.); Department of Energy/NNSA award no. DE-NA0003921 through the Consortium for Enabling Technologies and Innovation (ETI) (B.K. and C.F.-H.); CONICYT (Chilean National Commission for Scientific and Technological Research) through the Doctoral Fellowship program "Becas Chile," grant no. 72150387 (F. A. L.); and NSF CMMI Award 1400077 for Processing Mechanically Reliable Flexible Organic Electronic Films. **Author contributions:** Conceptualized work, acquired funding, managed project, and supervised students: C.F.-H. and B.K. Conducted investigations, verification, and data curation: Y.P., C.F.-H., W.-F.C., K.K., and F.A.L. Developed a methodology, conducted data analysis, developed software to acquire and analyze data, and wrote the original draft: Y.P. and C.F.-H. Conducted verification and data curation for the mechanical characterization of the samples: S.G., O.N.P., K.K., and Y.P. Reviewed and edited the manuscript: Y.P., C.F.-H., K.K., W.-F.C., F.A.L., O.N.P., S.G., and B.K. **Competing interests:** The authors declare that they have no competing interests. **Data and materials availability:** All data needed to evaluate the conclusions in the paper are present in the paper and/or the Supplementary Materials.

Submitted 2 June 2021
Accepted 26 October 2021
Published 15 December 2021
10.1126/sciadv.abj6565